Chinese Chemical Letters 33 (2022) 1577–1583

Contents lists available at ScienceDirect

Chinese Chemical Letters

journal homepage: www.elsevier.com/locate/cclet

A "cluster bomb" oral drug delivery system to sequentially overcome the multiple absorption barriers

Qingling Song[b,d,1], Huirui Wang[a,c,1], Junfei Yang[b,d], Hui Gao[b,d], Ke Wang[b,d], Hao Wang[b], Yun Zhang[b,d,e,*], Lei Wang[a,b,c,d,e,*]

[a] Luoyang Central Hospital Affiliated to Zhengzhou University, Luoyang 471009, China
[b] School of Pharmaceutical Sciences, Zhengzhou University, Zhengzhou 450001, China
[c] Tumor Immunity and Biomaterials Advanced Medical Center, Zhengzhou University, Luoyang 471009, China
[d] Henan Key Laboratory of Targeting Therapy and Diagnosis for Critical Diseases, Zhengzhou 450001, China
[e] Key Laboratory of Advanced Drug Preparation Technologies, Ministry of Education, Zhengzhou 450001, China

ARTICLE INFO

Article history:
Received 9 June 2021
Revised 18 August 2021
Accepted 24 August 2021
Available online 29 August 2021

Keywords:
Oral drug delivery
Absorption barrier
Cluster bomb
pH-sensitive
PePT1 receptor

ABSTRACT

Oral drugs have been widely used in clinical therapy, but their developments were severely limited by the side effects of drug exposure as well as the multiple biological barriers. In this study, we constructed a "cluster bomb" oral drug delivery system (DOX@PFeL@L100) with core-shell structure to overcome the complex absorption barriers. The inner core termed as "bomb" that contains a lot of ultra-small diameter Fe_3O_4 nanoparticles (DOX@PFeL NPs) loaded with doxorubicin (DOX) and modified with L-valine, which can efficiently penetrate the epithelial cells *via* PePT1 receptor mediated endocytosis. The outer shell of this "cluster bomb" is a layer of pH-sensitive polymer (Eudragit®L100) that can be served as a pH-responsive switch and effectively control the "bomb" release in the intestinal microenvironment to improve the antitumor efficiency by the Fenton like reaction of DOX and Fe^{2+}/Fe^{3+}. This study demonstrates that the "cluster comb" oral drug delivery system can sequentially overcome the multiple biological barriers, providing a safe and effective approach for tumor therapy.

Oral administration is the most widely accepted treatment approach in clinic due to its high safety, great convenience, and good patient acceptance [1]. However, the complicated gastrointestinal microenvironment, such as gastric acidity, various enzymes and intestinal mucus, remains the serious impediment to the adsorption of oral antitumor preparations [2-4]. In order to overcome these aforementioned problems, pH-sensitive microcapsules or microspheres are considered as an effective delivery method, which can remarkably prevent drug leakage under the stomach's acidic environment and release drugs in the intestine due to the suitable pH value [5-7]. Even so, it is still difficult to deliver drugs to the tumor sites efficiently. And the high concentration of released drug may destroy the physiological structure of intestine, leading to severe toxic side effects [8,9]. Notably, recent studies showed that drug loaded nanoparticles (NPs), smaller than 100 nm in size, are more beneficial for the intestinal biological barriers penetration and tumor distribution [10,11]. Unfortunately, only changing the NPs size is not enough to achieve a significant therapeutic effect. Therefore, the other effective means should be developed and utilized for improving the efficiency of oral drug delivery.

Enhancing the intestinal absorption is an important solution to improve the therapeutic effect of the oral drug delivery system [12,13]. Moreover, it has reported that transport proteins and receptor-mediated endocytosis of intestinal epithelial cells can specifically enhance the absorption efficiency of oral nano drugs [14,15]. For example, peptide transporter 1 (PepT1) on the surface of epithelial cells can improve epithelial affinity and intestinal permeability, which could effectively identify and transport amino acid and oligopeptide (di/tripeptide) modified preparations [16]. Some researchers claimed that NPs functionalized with L-valine (LV) could effectively target PepT1 receptor, increasing oral drugs delivery [17]. Interestingly, LV can also target to the large neutral amino acid transporter 1 (LAT-1) that overexpressed on the surface of breast cancer cells such as MCF-7 cells [18,19]. Inspired with the unique characteristics of LV, in this study, LV is used to enhance the NPs absorption by epithelial cells, subsequently leading to specific target to tumor cells.

* Corresponding authors.
E-mail addresses: zhang_yun@ymail.com (Y. Zhang), wanglei1@zzu.edu.cn (L. Wang).
[1] These two authors contributed equally to this work.

https://doi.org/10.1016/j.cclet.2021.08.113
1001-8417/

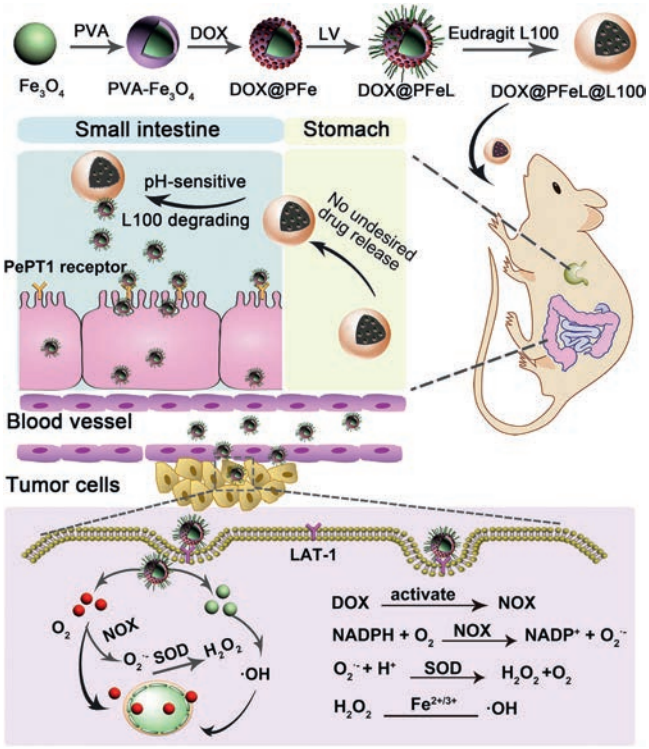

Scheme 1. Schematic illustration of the preparation of DOX@PFeL@L100 NPs and the mechanism of drug delivery *in vivo*.

In addition, delivering drugs precisely to the tumor sites is also critical to achieve a stronger anti-tumor effect [20]. Doxorubicin (DOX), as a broad-spectrum antitumor drug, has a strong cytotoxic effect leading to a wide range of biochemical effects in the body [21,22]. It has been proved that DOX can activate the nicotinamide adenine dinucleotide phosphate (NADPH) oxidase (NOX), triggering oxygen (O_2) to become a superoxide radical ($O_2^{\bullet-}$) and downstream H_2O_2, which is beneficial for Fe^{2+}/Fe^{3+} mediated Fenton reaction [23,24]. And the toxic hydroxyl radicals (·OH) generated by the above process could make oxidative damage to lipids, proteins and DNA of tumor cells, showing a promising combination strategy of DOX and Fe ions to increase the anti-tumor effect [25,26].

In this study, we have constructed a "cluster bomb" drug delivery system (DOX@PFeL@L100). As shown in Scheme 1, firstly, the Fe_3O_4 NPs with ultra-small particle size were prepared and modified with poly (vinyl alcohol) (PVA). Subsequently, DOX was loaded into PVA-modified Fe_3O_4 NPs (DOX@PFe) following with LV modification to construct DOX@PFeL NPs. Finally, DOX@PFeL NPs were encapsulated in the enteric microspheres (Eudragit®L100) by the solvent evaporation method to obtain the final formulation DOX@PFeL@L100. After oral administration, the Eudragit®L100 outershell can effectively maintain the formulation stability in the severe stomach acidic environment and prevent the drugs leakage before reaching the intestinal region. When DOX@PFeL@L100 reached the intestinal intact, the DOX@PFeL NPs were released to penetrate the intestinal barriers and further entered into blood circulation. During these barriers breaking process, LV was used to increase the epithelial affinity and permeability for achieving the superior intestinal epithelial penetration efficiency. After entering the bloodstream, DOX@PFeL NPs were accumulated to the tumor site due to the function of LV mediated tumor-targeting. Then, the combined therapy of DOX and Fe^{2+}/Fe^{3+} achieved the enhanced antitumor effect. In summary, this study provides a safe and reliable cluster bomb-like oral drug delivery system that can overcome multiple oral barriers and increase the accumulation of drugs at the tumor site to enhance the antitumor efficiency.

Ferumoxytol (Feraheme) is a supplements-iron that has been approved by the U.S. Food and Drug Administration (FDA) for the clinic treatments [27]. Notably, Fe_3O_4 NPs have been widely used in the basic biomedical scientific research for various drug delivery systems [28]. In this study, ultra-small Fe_3O_4 NPs were prepared by using a hydrothermal method [29]. As shown in Fig. 1A, a broad band at ~587 cm^{-1} was clearly observed in the FT-IR spectrum of Fe_3O_4 NPs, which was attributed to their Fe-O lattice pattern. Additionally, the magnetization curve of Fe_3O_4 NPs showed that the saturation magnetization is 49.7 emu/g, suggesting the good superparamagnetic property of Fe_3O_4 NPs (Fig. S1 in Supporting information). And the XRD pattern of Fe_3O_4 (Fig. 1B) showed six peaks corresponding to (220), (311), (400), (422), (511) and (440) Fe_3O_4 lattices, respectively, which further indicated that Fe_3O_4 NPs were successfully synthesized. And then the amount of PVA adsorbed on the Fe_3O_4 NPs was studied by thermogravimetric analysis (TGA). Studies have reported that when the pure PVA was heated to 600 °C, it will be completely degraded [30]. As shown in Fig. S2 (Supporting information), compared with Fe_3O_4, the weight of the PVA-Fe_3O_4 showed a remarkably loss of 11.2%, which could be attributed to the dehydration reaction of the -OH group in the PVA chain and the subsequent degradation of the CO_2 gas released by PVA. Moreover, the FTIR spectra also proved the attachment of PVA on the surface of Fe_3O_4 (Fig. S3 in Supporting information), which could be interpreted as the formation of hydrogen bonding force between PVA and Fe_3O_4 [31].

As shown in Fig. 1C, a characteristic peak of DOX at 485 nm was observed in the UV-vis absorption spectrum of DOX@PFe, indicating that DOX has been successfully loaded into PVA-Fe_3O_4 NPs. The band was observed at 804 cm^{-1} in pure DOX due to N–H fluctuations decreases in the FTIR spectrum in DOX@PFe (Fig. S4 in Supporting information). It can be explained that the -NH_2 of DOX and the -OH group of PVA were attached to the PVA-Fe_3O_4 NPs through hydrogen bonding interaction. This is consistent with previous reports [30]. Then, we also evaluated the drug release properties of DOX@PFeL@L100 at different pH values. The result showed that DOX was hardly released at pH 1.2, pH 5.5 and pH 7.4 (Fig. 1D and Fig. S5 in Supporting information). However, an increasing release rate was apparently observed at pH 6.8 due to the pH sensitivity of Eudragit®L100. We also investigated the release effect of DOX@PFeL in the simulated tumor pH environment (pH 5.5 + 5 mmol/L H_2O_2). Finally, the release rate of DOX was 60.10% after 48 h incubation. TEM images (Fig. 1E) of Fe_3O_4, PVA-Fe_3O_4, DOX@PFe and DOX@PFeL NPs all showed regular spherical shape. And as shown in Fig. 1F, the DOX@PFeL NPs had a hydration particle size of 84.6 ± 3.2 nm and a zeta potential of 4.2 ± 1.2 mV. As depicted in Fig. 1G, the DOX@PFeL@L100 delivery system had the particle size of ~4 μm, and the DOX@PFeL NPs can be clearly observed in the partially enlarged image. In addition, the changes of zeta potential value of LV in different pH environments indicate that the pH 8 environment is more conducive to the electrostatic adsorption of LV on the surface of positively charged NPs (Fig. S6 in Supporting information).

As shown in Fig. S7 (Supporting information), there was no obvious UV absorption at 485 nm when the PVA-Fe_3O_4 mixed with HCl, which indicated that HCl would hardly affect the detection of DOX content. The loading efficiency of DOX in DOX@PFeL and DOX@PFeL@L100 NPs was 13.19% ± 2.12% and 0.86% ± 0.21%, respectively, which can meet the requirements of subsequent experiments. Furthermore, the ability of drug protection and controlled release of the formulation play an important role for the drug delivery at different conditions. The confocal laser scanning microscope (CLSM) was used to evaluate the morphology of DOX@PFeL@L100 under different pH conditions. As shown in

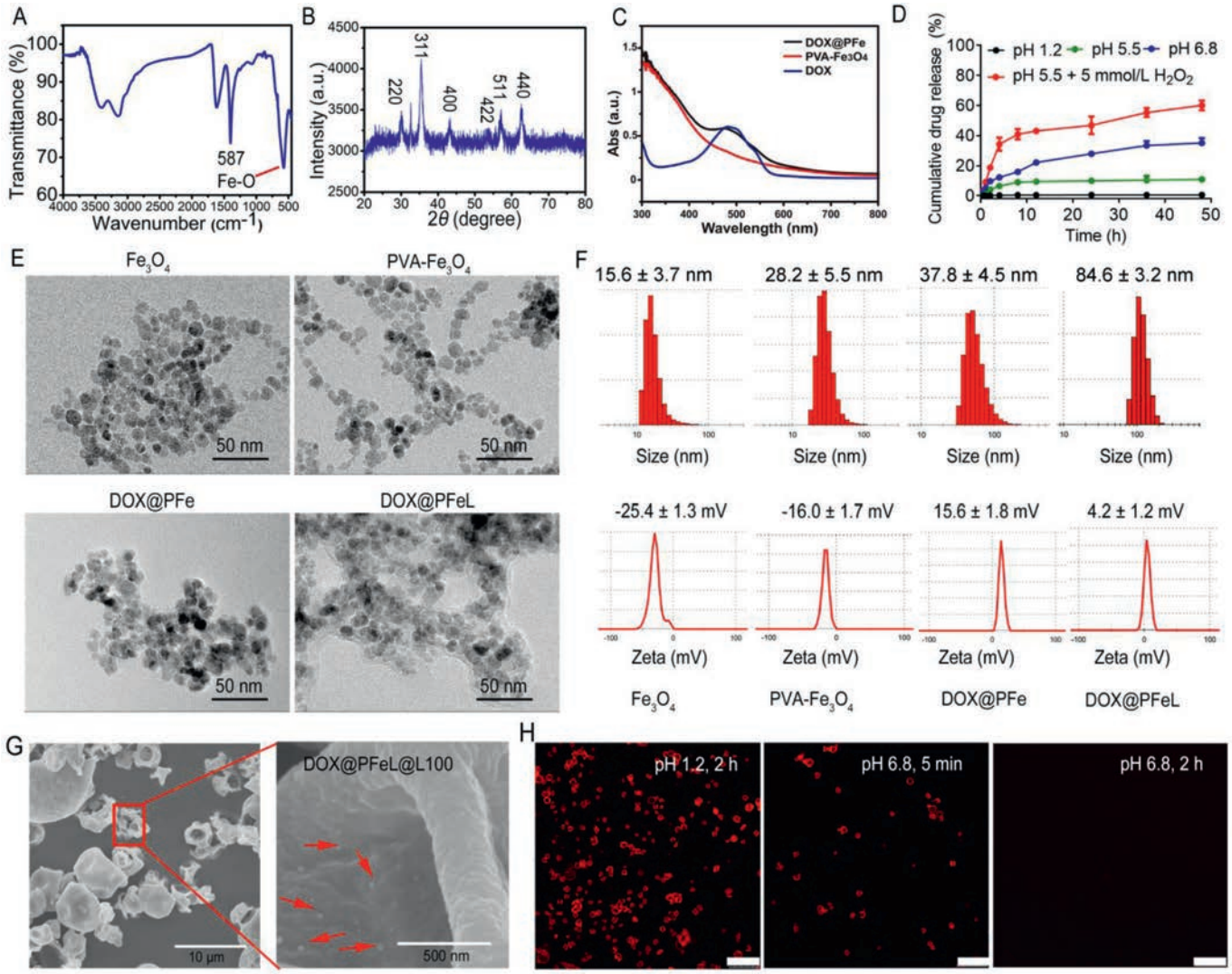

Fig. 1. Preparation and characterization of DOX@PFeL@L100. (A) FTIR spectra of Fe_3O_4 NPs. (B) XRD spectrum of the Fe_3O_4 NPs. (C) UV-vis spectra of DOX, Fe_3O_4, and DOX@PFe, respectively. (D) *In vitro* drug release profiles of DOX@PFeL@L100 in different conditions ($n = 3$). (E) The TEM images and (F) size distribution and zeta potential of Fe_3O_4 NPs, PVA-Fe_3O_4, DOX@PFe and DOX@PFeL, respectively. (G) SEM images of DOX@PFeL@L100. (H) The CLSM images of DOX@PFeL@L100 in different pH environment (the red fluorescence was attributed to DOX). Scale bar: 25 μm.

Fig. 1H, DOX@PFeL@L100 still maintained the integrity of the shape when it was incubated with the simulated gastric fluid (pH 1.2) for 2 h. However, the morphology of DOX@PFeL@L100 was destroyed and disintegrated quickly once the pH value was increased to 6.8 (simulated intestinal fluid). Of note, after 2 h incubation, the CLSM images showed the background color, which suggested that DOX@PFeL NPs were released completely.

The Caco-2 cellular uptake behaviors of different preparations were evaluated by CLSM after being incubated for 0.5 h, 1 h and 2 h, respectively, and the co-localization ratios were also calculated (Figs. 2A and B). After incubation for 0.5 h, there were no significant differences in fluorescence intensity among all the groups. With the extension of incubation time, the red fluorescence intensity was clearly increased in all groups. After incubation for 2 h, the strongest fluorescence intensity was observed in DOX treatment group. This phenomenon was mainly because DOX was easily uptaken due to its natural characteristics such as positive polarity and small molecule structure. Surprisingly, there were significant differences between DOX@PFeL and DOX@PFe treatment group, indicating that these NPs can be effectively uptaken by Caco-2 cells due to the targeting function of LV. Furthermore, the Gly-Sar, as the inhibitor of PePT1 receptor, was pre-incubated with Caco-2 cells for 30 min for further determining the targeting function of LV. It can be seen that the cell uptake rate was significantly reduced in the DOX@PFeL + Gly-Sar group, which proved that LV receptor-mediated endocytosis could promote the intestinal epithelial cell penetration of NPs. In addition, the free carrier materials in the preparation were non-toxic to Caco-2 cells and would not cause damage to the intestinal tract (Fig. 2C).

Firstly, the Fe_3O_4 NPs were co-cultured with Caco-2 cells for 2 h, and then TEM was used to observe the behavior and integrity of Fe_3O_4 NPs. As shown in Fig. S8 (Supporting information), Fe_3O_4 NPs could maintain their complete shape after being uptaken by Caco-2 cells. Subsequently, the efficiency of epithelial transport was further investigated by the Transwell method (Fig. 2D). The results showed that DOX@PFeL NPs can penetrate the Caco-2 cell monolayer and increase the drug amount of basolateral side compared with the DOX@PFeL+Gly-Sar group ($P < 0.05$) (Fig. 2F). Therefore, the efficiency of transepithelial transport of DOX@PFeL NPs can be improved by protein receptor-mediated transport. At the same time, the TEER values of different preparations showed almost visible changes before and after incubation

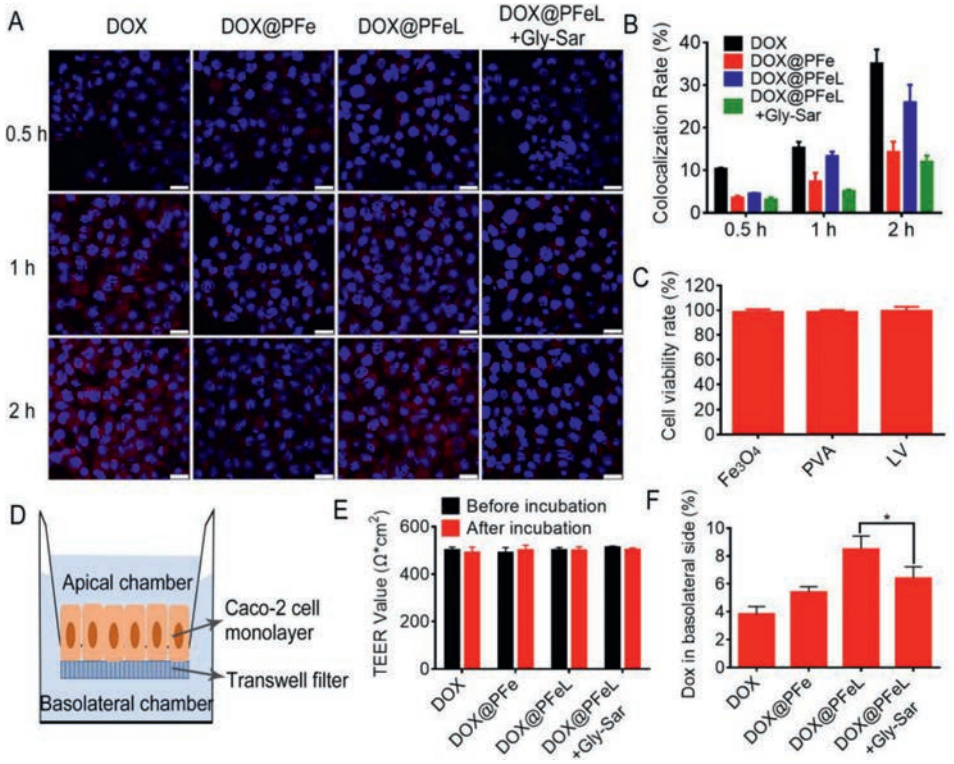

Fig. 2. Studies of cellular uptake and transepithelial transport of different groups. (A) Caco-2 cell uptake of different groups (Scale bar: 25 μm). (B) Caco-2 cell co-localization rate of different groups ($n = 3$). (C) Cell viability rate of Caco-2 by different concentrations of blank vector. (D) The construction of Caco-2 cell monolayer. (E) TEER values of Caco-2 cell monolayers before and after incubation ($n = 3$) and (F) Transepithelial transport ($n = 3$). $^*P < 0.05$.

(Fig. 2E), suggesting that the formulation was transported across cells rather than disrupting the cell layers. Moreover, the intact nanoparticles were observed in basolateral chamber, which indicated that DOX@PFe and DOX@PFeL NPs had good stability when they were transported across the epithelium (Fig. S9 in Supporting information).

The efficiency of tumor cell uptake is critical to the therapeutic effect of drugs. The cellular uptake behavior of NPs was evaluated by using CLSM. As shown in Fig. 3A, the nuclei were stained blue fluorescence by DAPI, while NPs were localized by DOX signals (red fluorescence). It can be seen that the DOX-treated group had the highest uptake rate at each time point, because DOX is a small molecule preparation that is easily uptaken by cells. Therefore, we have modified the drug with functional groups to improve the effect of DOX crossing the gastrointestinal barrier. The cellular uptake effects of all groups were enhanced with the prolonged incubation time. However, the red fluorescence of DOX@PFeL group has stronger red fluorescence after 4 h incubation. This result was because LV can target LAT-1 receptor which is overexpressed on the surface of MCF-7 cells [32]. As shown in Fig. 3B, the results were consistent with the CLSM results, indicating that NPs can be uptaken by MCF-7 cells.

Cytotoxicity studies with different concentrations of Fe_3O_4 and PVA-Fe_3O_4 were performed in MCF-7 cells for 24 h (Fig. S10 in Supporting information). With the increasing of Fe concentration, the cell viability of MCF-7 cells was not significantly changed until 2000 μmol/L, suggesting that the drug carrier system had good biocompatibility. As shown in Fig. S11 (Supporting information), the DOX@PFeL NPs had the highest inhibition effect, suggesting that the preparation can achieve better anti-tumor efficiency. As shown in Fig. 3C, the apoptosis rates of the DOX, Fe_3O_4, DOX@PFe and DOX@PFeL groups were 40.6% ± 2.9%, 10.9% ± 1.4%, 42.5% ± 1.9% and 46.4% ± 2.2%, respectively. These results indicated that the functional NPs modified with LV can achieve the same anti-tumor effect as DOX.

Furthermore, we selected DCFH-DA as an indicator to detect ROS produced by different preparations in cells to evaluate the related research at cellular level. Non-fluorescent DCFH can be oxidized by alkyl radicals into fluorescent DCF; the more intracellular ROS, the stronger the green fluorescence. As shown in Fig. 3D, the Control group and the DOX group produced negligible green fluorescence while the DOX@PFeL group produced the brightest green fluorescence. These results indicated that DOX had a positive effect on iron-mediated ROS production.

To further evaluate the intestinal absorption and circulation of different groups, we conducted an evaluation in animals. All animal experiments were strictly conducted according to the guidelines stipulated and approved by Henan Laboratory Animal Center. As shown in Fig. 4A, the intestinal epithelial tissue of saline group had no fluorescence, while the corresponding DOX@L100 and DOX@PFe groups were detected weak fluorescence signals. This phenomenon can be explained as follows: drugs and nano preparations have strong positive charge and are easily removed by intestinal mucus. Of note, the strong red fluorescence signal (DOX) was detected in the villi and epithelial cells after being treated with DOX@PFeL. These results further indicated that DOX@PFeL could improve transepithelial transport through the oligopeptide transporter pathway, which was consistent with the *in vitro* results. In addition, the study of intestinal circulation in rat model was used to further verify the intestinal adsorption effect of different preparations (Fig. 4B). As shown in Fig. 4C, the drug absorption rate of the DOX@PFeL group was 57.18% ± 3.01% during 4 h cycle, which was higher than the free DOX group ($P < 0.01$). The plasma concentration time curves and pharmacokinetic parameters are shown in Figs. 4D and E. Compared with the control group, the C_{max} value of DOX@PFeL@L100 treated group was

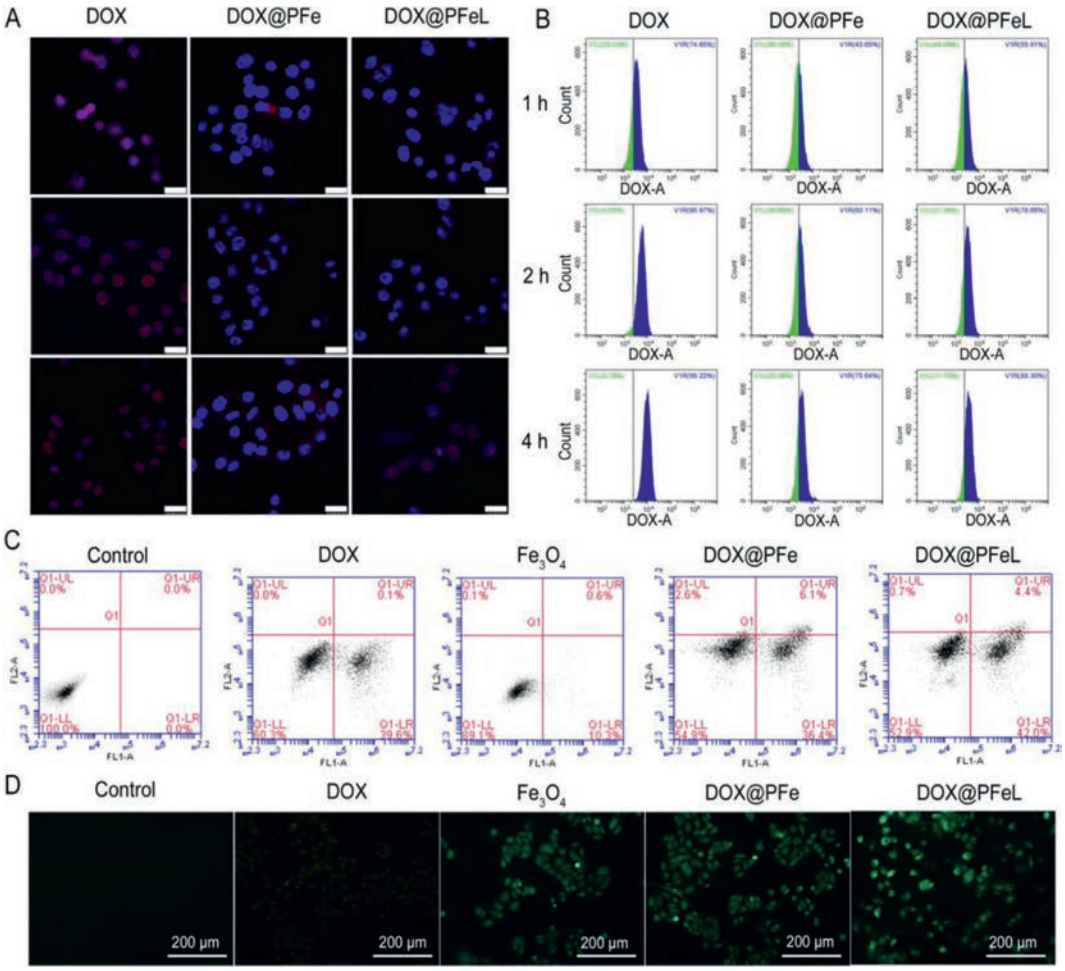

Fig. 3. Cytotoxicity and cell uptake analysis. MCF-7 cell uptake was detected by (A) CLSM and (B) flow cytometry after being treated with different groups for 1, 2, and 4 h, respectively (Scale bar: 25 μm). (C) Cell apoptosis of MCF-7 cells for 24 h. (D) DCFH-DA probe detection of intracellular ROS in different groups (Scale bar: 200 μm).

0.50 ± 0.13 μg/mL, which was higher than that of the other treatment groups. Notably, the DOX@PFeL@L100 treated group achieved the highest relative bioavailability (F_{rel}), which was 5.9-fold higher than the values obtained by the DOX treatment. Taken together, DOX@PFeL@L100 with the superior mucus-penetrating and cellular uptake capabilities could be served as a valuable drug delivery system, improving the drugs bioavailability. Additionally, the biodistribution of DOX in heart tissues was further detected by HPLC after oral treatment according to the previously reported method [33]. Furthermore, as shown in Fig. S12 (Supporting inforamation), the DOX concentration of heart tissues in DOX@PFeL@L100 treated group was significantly lower than that of the other three groups, respectively. This result suggested that this DOX delivery system can decrease the DOX concentration in heart, reducing cardiac toxicity.

Subsequently, the *in vivo* distribution of IR780 labeled preparations at different time points was detected by real-time NIR fluorescence imaging. As shown in Figs. 5A and B, the IR780@PFeL@L100 treatment group exhibited a stronger fluorescence signal than that of the other treatment group in tumor site at 24 h and remained obvious fluorescence until 48 h, indicating that more IR780@PFeL@L100 was delivered to the tumor site and had the highest tumor distribution. However, the free IR780 group and IR780@L100 group were mainly distributed in the stomach and small intestine, with only a small amount at the tumor site. In addition, we also examined the fluorescence intensity of the major organs tissues in each group. As shown in Figs. 5C and D, the DOX@PFeL@L100 group had the highest tumor distribution, which was consistent with the real-time fluorescence distribution results. These above results all suggested that: i) Microcarriers can pass through the gastrointestinal tract without being degraded by gastric acid for the protection of Eudragit®L100. ii) LV can effectively improve the intestinal absorption and tumor targeting ability of NPs.

In order to investigate the therapeutic efficacy of DOX@PFeL@L100 after oral administration, the subcutaneous mice model was established with MCF-7 tumor cells. The tumor size of each mouse was measured to monitor the therapeutic effect. As shown in Fig. 6A and Fig. S13 (Supporting information), compared to mice treated with Fe_3O_4@L100 or saline groups, the significant reduction in tumor size was observed in DOX@PFeL@L100 (20 mg/kg) treatment group. Moreover, there was almost no tumor suppressive effect in the DOX@PFeL group, which may be attributed to the degradation of DOX@PFeL in the gastric acid environment. This result also suggested that Eudragit®L100 could effectively resist the gastric acid environment. Additionally, there was almost no visible weight change in the treatment groups, indicating no significant toxic effects (Fig. 6B). H&E staining of tumor tissues in the saline group showed low cell nuclear quality, uniform nucleus and tightly arranged tissues, indicating malignant proliferation of tumor tissues. However, a large area of tumor cell necrosis, nuclear shrinkage, fragmentation or lysis was observed in the DOX@PFeL@L100 group, which suggested that it had a better antitumor effect *in vivo*. As shown in Fig. 6C, H&E staining

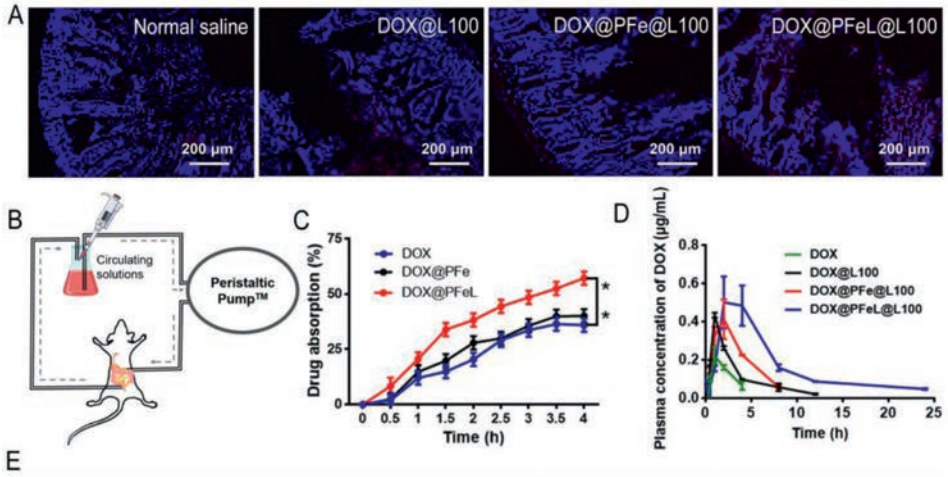

E

Parameter	Unit	DOX	DOX@L100	DOX@PFe@L100	DOX@PFeL@L100
$t_{1/2}$	h	1.66	2.45	3.14	3.16
t_{max}	h	1.00	1.00	2.00	2.00
C_{max}	μg/mL	0.22 ± 0.04	0.43 ± 0.12	0.32 ± 0.06	0.50 ± 0.13
AUC_{0-t}	μg/mL*h	0.52 ± 0.14	1.22 ± 0.24	1.31 ± 0.18	3.07 ± 0.82
F_{rel}	%	100	235	252	590

Fig. 4. *In situ* intestinal absorption and anti-tumor efficiency *in vivo*. (A) The fluorescence images of intestine after administration of different groups for 4 h (Scale bar: 200 μm). (B) Schematic illustration of *in situ* intestinal perfusion device model. (C) *In situ* intestinal circulation of different formulations. (D) Plasma concentration of different DOX formulations after oral administration. (E) Pharmacokinetic parameters of different formulations following oral administration (The rats were orally administrated with different groups in a dose equivalent to 20 mg/kg of Dox.).

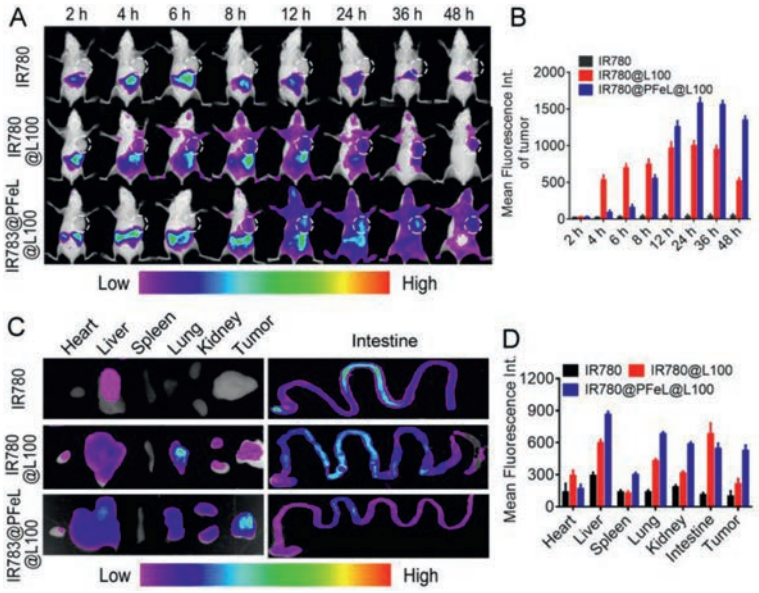

Fig. 5. *In vivo* NIR fluorescence imaging. (A) Images of time-dependent whole-body imaging of mice after oral administration of different groups after oral administration for 48 h. (B) The mean fluorescence intensity of tumor at the different time. (C) *Ex vivo* optical images of tissues and organs of mice sacrificed at 48 h after oral administration. (D) Fluorescence values of major organs of sacrificed at 48 h after oral administration.

of intestine showed that the intestinal epithelium and intestine wall of each treatment group had no obvious lesions. Additionally, H&E staining of major organs, such as heart, liver, spleen, lung and kidney, showed no noticeable organ damage in the treatment group (Fig. S14 in Supporting information), indicating that the excellent biocompatibility and almost negligible toxicity of DOX@PFeL@L100. The TUNEL assay was also used to further evaluate the apoptosis profile of tumor tissue. There were few markers of apoptosis in the control group and the Fe_3O_4 group. However, the DOX@PFeL@L100 group had higher apoptosis than the other treatment groups, which was consistent with the H&E staining result. In summary, DOX@PFeL@L100 NPs can efficiently pass the intestinal environment through pH-sensitive material. Moreover, the surface modified with LV was also helpful for NPs to penetrate intestinal epithelial cells and deliver DOX to the tumor sites, leading to a superior treatment effect.

In summary, a “cluster bomb” oral drug delivery system has been successfully prepared, which can effectively overcome the

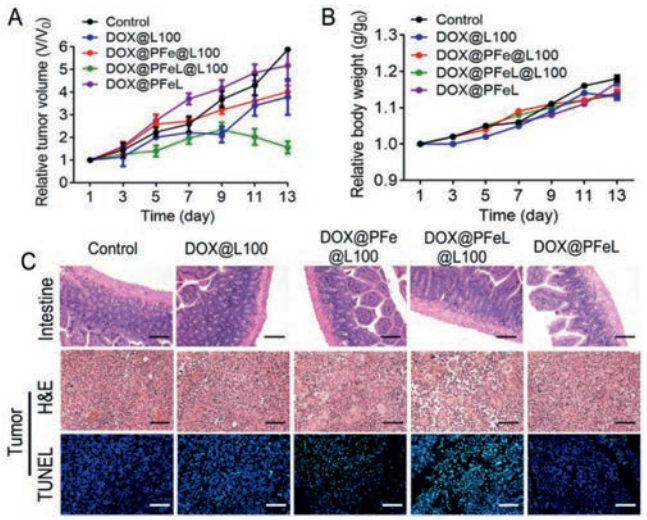

Fig. 6. *In vivo* antitumor efficacy. (A) Changes in relative tumor volume and (B) body weight during the different treatments. (C) H&E staining (Scale bar: 400 μm) and TUNEL examination of tumor sections by immunofluorescence (Scale bar: 50 μm) in different groups ($n = 5$).

oral absorption barriers and specifically target tumor sites. First, the outershell Eudragit®L100 of DOX@PFeL@L100 can prevent the nanoparticles from being degraded by gastric acid and protect the DOX@PFeL NPs to be transported to the intestinal environment efficiently. Then, surface modified with LV was used to overcome epithelial barrier, and subsequently deliver drugs into the blood circulation. Finally, LV can efficiently target to tumor cells, achieving a highly anti-tumor effect. *In vitro* and *in vivo* evaluation have proved that this "cluster bomb" oral drug delivery system has some advantages in the following aspects: i) penetration of multiple absorption barriers; ii) good bioavailability; iii) high accumulation to tumor sites and superior anti-tumor effect. More importantly, based on the high concentration of H_2O_2 at the tumor microenvironment, the Fe ion and DOX were co-delivered by DOX@PFeL to the tumor sites, which could significantly enhance the anti-tumor efficiency. Compared with free drugs and conventional drug delivery systems, our formulations can sequentially overcome multiple oral absorption barriers, providing a safe and effective oral anti-tumor drug delivery strategy.

Declaration of competing interest

The authors declare no conflict of interest.

Acknowledgments

This work was supported by the National Natural Science Foundation of China (Nos. 81773276, 81972907, 81874304, and U1804183), Key Scientific Research Project (Education Department of Henan Province) (No. 20HASTIT049) and Modern Analysis and Computer Center of Zhengzhou University.

Supplementary materials

Supplementary material associated with this article can be found, in the online version, at doi:10.1016/j.cclet.2021.08.113.

References

[1] M. Duran-Lobato, Z. Niu, M.J. Alonso, Adv. Mater. 32 (2020) 1901935.
[2] P. Lundquist, P. Artursson, Adv. Drug Deliv. Rev. 106 (2016) 256–276.
[3] Z. Zhang, Y. Lu, J. Qi, W. Wu, Acta Pharm. Sin. B 11 (2021) 2449–2468.
[4] S. Zhao, J. Li, F. Wang, et al., Chin. Chem. Lett. 31 (2020) 1147–1152.
[5] S.H. Lee, J.G. Song, H.K. Han, J. Control. Release 311 (2019) 74–84.
[6] W. Li, Y. Li, Z. Liu, et al., Biomaterials 185 (2018) 322–332.
[7] Y. Wang, X. Wang, J. Zhang, et al., Chin. Chem. Lett. 30 (2019) 885–888.
[8] C.Y. Wong, H. Al-Salami, C.R. Dass, Int. J. Pharmaceut. 537 (2018) 223–244.
[9] S.H. Kang, V. Revuri, S.J. Lee, et al., ACS Nano 11 (2017) 10417–10429.
[10] F. Xia, W. Fan, S. Jiang, et al., ACS App. Mater. Inter. 9 (2017) 21660–21672.
[11] B. Wang, Y. Zhai, J. Shi, et al., J. Control. Release 268 (2017) 225–236.
[12] X. Zhu, J. Wu, W. Shan, et al., Adv. Funct. Mater. 26 (2016) 2728–2738.
[13] Y. Liu, Z. Jiang, X. Hou, et al., Nanomed. Nanotechnol. 21 (2019) 102075.
[14] Q. Song, J. Jia, X. Niu, et al., Nanoscale 11 (2019) 15958–15970.
[15] Q. Song, C. Zheng, J. Jia, et al., Adv. Mater. 31 (2019) e1903793.
[16] Y. Sun, W. Gan, M. Lei, et al., Asian J. Pharm. Sci. 13 (2018) 555–565.
[17] B. Gourdon, C. Chemin, A. Moreau, et al., Int. J. Pharmaceut. 529 (2017) 357–370.
[18] L. Li, X. Di, M. Wu, et al., Nanomed. Nanotechnol. 13 (2017) 987–998.
[19] Z.Y. Ong, S. Chen, E. Nabavi, et al., ACS App. Mater. Inter. 9 (2017) 39259–39270.
[20] X. Li, Y. Zhang, Z. Ma, et al., Chin. Chem. Lett. 30 (2019) 489–493.
[21] A. Sharma, E.J. Kim, H. Shi, et al., Biomaterials 155 (2018) 145–151.
[22] L. Wang, P. Zhang, J. Shi, et al., ACS App. Mater. Inter. 7 (2015) 5736–5747.
[23] Y. Ding, J. Wan, Z. Zhang, et al., ACS App. Mater. Inter. 10 (2018) 4439–4449.
[24] W. Bao, X. Liu, Y. Lv, et al., ACS Nano 13 (2019) 260–273.
[25] Y. Dai, Z. Yang, S. Cheng, et al., Adv. Mater. 30 (2018) 1704877.
[26] Y. Liu, W. Zhen, L. Jin, et al., ACS Nano 12 (2018) 4886–4893.
[27] V. Trujillo-Alonso, E.C. Pratt, H. Zong, et al., Nat. Nanotechnol. 14 (2019) 616–622.
[28] C. Shasha, K.M. Krishnan, Adv. Mater. 33 (2020) e1904131.
[29] L. Wang, P. Zhang, J. Shi, et al., ACS App. Mater. Inter. 7 (2015) 5736–5747.
[30] S. Kayal, R.V. Ramanujan, Mater. Sci. Eng. C 30 (2010) 484–490.
[31] W. Zhang, R. Taheri-Ledari, Z. Hajizadeh, et al., Nanoscale 12 (2020) 3855–3870.
[32] A.E. Porter, ACS App. Mater. Inter. 9 (2017) 39259–39270.
[33] L. Wang, J. Shi, X. Jia, et al., Pharm. Res. 30 (2013) 2757–2771.